Preliminary Quasar Model Based on the Yilmaz Exponential Metric

Roger E. Clapp
Basic Research Associates, Incorporated, Cambridge, Massachusetts 02138
(Received 15 April 1971; revised manuscript received 6 April 1972)

A partially collapsed spherical matter distribution is analyzed with the aid of an integral equation for the gravitational potential, derived from the Yilmaz exponential metric. This metric equals the Schwarzschild metric for weak gravitational fields but differs for strong fields, avoiding any catastrophic collapse into a black hole. The quasars are interpreted as gravitationally compacted protogalaxies, with galactic masses and dimensions which are initially stellar but increase as the quasar evolves into a galaxy. Good agreement is found between the surface red shifts calculated from the preliminary quasar model and the observed red shifts for a sample of 151 quasars. Thus the quasar red shifts can be interpreted as primarily of gravitational rather than cosmological origin, and the quasars are placed at moderate distances, 3C48 being within the local group of galaxies.

I. INTRODUCTION

The Yilmaz exponential metric gives the same results for the "four tests" as the Schwarzschild metric, but differs from the Schwarzschild metric in that it has no Schwarzschild singularity and is readily generalized to incorporate multiple sources and distributed sources for the gravitational field. The generalization of the static-limit exponential metric to incorporate moving sources and time-dependent fields can probably be carried out in several alternative ways, but this kind of generalization will not be needed in the present calculation.

As originally presented by Yilmaz,[1] the exponential metric was obtained from a scalar-field theory of gravitation. In his second version, Yilmaz[2] obtained the same metric from a tensor-field theory.

Objections to the Yilmaz scalar and tensor theories have been raised by Will and Nordtvedt,[3] and by Kinnersley.[4] In the static limit, however, we need not be concerned with these difficulties.

In the static limit, the exponential metric has the form

$$ds^2 = e^{-2u}c^2dt^2 - e^{2u}(dx^2+dy^2+dz^2), \tag{1}$$

where

$$u = \sum_j u_j = \frac{GM_1}{c^2 r_1} + \frac{GM_2}{c^2 r_2} + \frac{GM_3}{c^2 r_3} + \cdots . \tag{2}$$

The M_j are gravitational sources, and the r_j are the distances from these sources to the point at which the gravitational potential u is being specified. The observer is outside the influence of the sources in (2), in a region where u is effectively zero, and the velocity of a massless particle equals c. For regions nearer the sources, this velocity slows to ce^{-2u}.

When only one of the terms in (2) is varying significantly over the region of interest, a transformation can be introduced which has the effect of moving the observer into the field of the other terms, where his scale of space, scale of time, and scale of gravitational mass are altered. In the metric (1) the product $dt\exp(-u_2-u_3-\cdots)$ is replaced by a redefined dt, while $dx\exp(u_2+u_3+\cdots)$ becomes the new dx, and so forth. What remains is then a metric of the same form (1), but with only a single term in the expression for the gravitational potential,

$$u = \frac{GM}{c^2 r}, \tag{3}$$

in which

$$r = r_1\exp(u_2+u_3+\cdots), \tag{4}$$

$$M = M_1\exp(u_2+u_3+\cdots). \tag{5}$$

The transformation (5) can be interpreted as a gravitational violet shift or blue shift, applied to the gravitational radiation from the source M_1 to the observer. Since the observer is now within the gravitational potential field of the other sources, gravitons and photons and neutrinos will fall toward him and have their energies increased. The source M_1 thus appears stronger to him, now having the effective magnitude M given in (5).

However, the observer has remained outside the gravitational field of M_1, so that gravitons leaving M_1 are red-shifted in climbing from M_1 to the observer, against this gravitational force. For this observer, therefore, the effective gravitational mass in M_1 is less than the sum of the gravitational

masses of the individual atoms in M_1. In gathering together, these atoms have made it more difficult for gravitons to leave.

This factorization of the metric is unique to the exponential metric, and is an argument in favor of its use to replace the Schwarzschild metric. For a single source the exponential metric matches the isotropic form of the Schwarzschild metric,[5]

$$ds^2 = \frac{(1-\frac{1}{2}u)^2}{(1+\frac{1}{2}u)^2}c^2\,dt^2 - (1+\tfrac{1}{2}u)^4(dx^2+dy^2+dz^2), \quad (6)$$

to three terms in the temporal part and two terms in the spatial part, when the dependence on u in (1) and (6) is expressed in terms of power-series expansions. This match is sufficient to give identical results for the "four tests," which are all weak-field tests in which u is much smaller than unity.

Thus the solar system tests cannot distinguish between (1) and (6). We can look to strong-field phenomena, where (1) is well behaved but (6) becomes singular, for a "fifth test" which might provide the experimental evidence needed to distinguish between the predictions of the exponential metric and the predictions of the Schwarzschild metric.

II. FIFTH TEST

Evidence is accumulating[6] that certain quasars are closely associated with galaxies of much smaller red-shift values. For these quasars at least, the quasar red shifts cannot be entirely cosmological, but may be gravitational in origin if the quasar is a highly compacted structure. In one particular case,[7] there is evidence that a quasar which is close to a galaxy has produced a tidal distortion of that galaxy, suggesting that the quasar mass is not much smaller than a galactic mass.

In the quasars, therefore, we may have examples of structures with strong gravitational fields, galactic masses compacted to dimensions comparable to supergiant stars. This would put the matter distribution close to or within its Schwarzschild radius, where the Schwarzschild metric (6) predicts singular behavior such as catastrophic gravitational collapse into a "black hole." The Yilmaz exponential metric (1), on the other hand, is well behaved for a highly compacted matter distribution. We will examine its predictions of the properties of such a matter distribution, to determine whether these predicted properties resemble the observed properties of the quasars. If they do, then we may be able to say that the explanation of quasar properties constitutes a *fifth test* of a gravitational theory, a strong-field test which other theories will need to confront.

In order to isolate the features of a compacted matter distribution which are specifically associated with the choice of the metric, from other features which are associated with the kinetics and thermodynamics of the particular matter that is present, we will treat a very simple model, a spherical matter distribution with constant intrinsic density and with a sharp boundary. This is then a preliminary quasar model, which can later be generalized through the introduction of a thermodynamic equation of state, with self-consistent distribution functions of pressure, density, and temperature, with energy generation in the appropriate thermonuclear reactions.

A generalization to incorporate internal rotations will also be needed, once the static-limit formulation has been clarified. However, the form of this generalization need not be specified for the present calculation. We can proceed in terms of a simple scalar gravitational potential function, $u(r)$, depending only on the radial distance from the center of the spherical mass distribution.

III. INTEGRAL EQUATION

In the Yilmaz theory, a distribution of gravitational waves will make a contribution as a gravitational source, and a real quasar can be expected to generate such a distribution. However, the static-limit analysis assumes that gravitational waves are not present, and that the actual matter distribution in the spherical model represents the only gravitational source.

A *constant intrinsic density* is assumed in this model. This is the density as it would appear to an observer located in the midst of the mass distribution. To an observer outside the gravitational field, a region with the intrinsic density ρ and the gravitational potential u will appear to be compacted by the linear compaction factor e^{-u}, as obtained from (1). The apparent density is thus increased to ρe^{3u}. Locally, however, the reduction in the separation of the atoms is accompanied by a reduction in the diameter of each atom, to give no locally apparent density change.

While ρe^{3u} is the density value to use when we compute the number of atoms in a compacted region, a different expression is needed when we compute the effect of the atoms as gravitational sources. Here we need to include a red-shift factor, e^{-u}, which reduces the effective source strength to

$$\rho'(r) = \rho e^{2u(r)}. \quad (7)$$

We can subdivide the spherical source distribution into concentric shells, each of thickness dr''.

The effective gravitational mass of a shell at the radius r'' will be given by

$$dM'' = 4\pi\rho'(r'')r''^2 dr'' . \tag{8}$$

From a summation over the atoms in this shell, in accordance with (2), we find the contributions of (8) to the potential function, outside and inside the shell, to be

$$du(r) = \frac{G\,dM''}{c^2 r} \quad \text{for} \quad r > r'' , \tag{9}$$

$$du(r) = \frac{G\,dM''}{c^2 r''} \quad \text{for} \quad r < r'' . \tag{10}$$

We can now sum these contributions for a spherical mass distribution of radius R. Outside the sphere the resulting potential function is

$$u(r>R) = \frac{4\pi G}{c^2 r}\int_{r''=0}^{r''=R} \rho'(r'')r''^2 dr'' . \tag{11}$$

Inside the mass distribution, $u(r)$ is given by

$$u(r<R) = \frac{4\pi G}{c^2 r}\int_{r''=0}^{r''=r} \rho'(r'')r''^2 dr'' + \frac{4\pi G}{c^2}\int_{r''=r}^{r''=R} \rho'(r'')r''\,dr'' . \tag{12}$$

At the center of the sphere, (12) reduces to

$$u(0) = \frac{4\pi G}{c^2}\int_{r''=0}^{r''=R} \rho'(r'')r''\,dr'' . \tag{13}$$

When (13) is subtracted from (12), and (7) is used, an integral equation for $u(r)$ is obtained:

$$u(r<R) = u(0) - \frac{4\pi G\rho}{c^2} \times \int_{r''=0}^{r''=r} e^{2u(r'')}\left(r'' - \frac{r''^2}{r}\right)dr'' . \tag{14}$$

The integral equation (14) can be written in a dimensionless form with the aid of the definitions

$$L = c(4\pi G\rho)^{-1/2} e^{-u(0)} , \tag{15}$$

$$s = r/L , \quad s'' = r''/L , \quad S = R/L , \tag{16}$$

$$\zeta(s) = e^{u(Ls)-u(0)} . \tag{17}$$

It is most convenient to let $\zeta^2(s)$ be the function to be determined, and the integral equation then takes the form

$$-\log_e \zeta^2(s) = \int_{s''=0}^{s''=s} \zeta^2(s'')\left(2s'' - \frac{2s''^2}{s}\right)ds'' . \tag{18}$$

This dimensionless integral equation can be solved by a power-series expansion:

$$\zeta^2(s) = C_0 + C_2 s^2 + C_4 s^4 + \cdots , \tag{19}$$

$$C_0 = 1, \quad C_2 = -\tfrac{1}{3}, \quad C_4 = \tfrac{4}{45} , \tag{20}$$

and so forth, as determined with the help of the power-series expansion for $\log_e(1+x)$. For the actual calculations, these coefficients were evaluated through C_{16}.

From Eq. (19) and the power-series expansion for $(1+x)^{3/2}$ a related series can be obtained:

$$\zeta^3(s) = D_0 + D_2 s^2 + D_4 s^4 + \cdots , \tag{21}$$

with

$$D_0 = 1, \quad D_2 = -\tfrac{1}{2}, \quad D_4 = \tfrac{7}{40} , \tag{22}$$

and so forth. These coefficients were evaluated through D_{16} for the present calculation.

The function $\zeta^2(s)$ is a positive function which equals unity for $s = 0$, and which decreases monotonically toward zero as s increases toward positive infinity. For large values of s, this asymptotic behavior of the function means that the integral in (18) will be dominated by contributions from values of s'' which are much smaller than s. This suggests the asymptotic replacement

$$\left(2s'' - \frac{2s''^2}{s}\right) \sim 2s'' , \tag{23}$$

giving, as the asymptotic solution to (18),

$$\zeta^2(s) \sim s^{-2} , \tag{24}$$

which will accordingly be valid only for large values of s.

The series (19), truncated at the C_{16} term, can give useful numerical results for rather large values of the argument s, provided the delta-square summation technique[8,9] is used, not just once but iterated as many times as possible, which is four times for the nine-term truncated series. Figure 1 shows the results obtained from the truncated

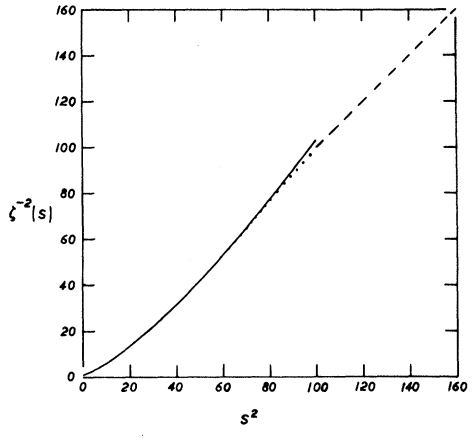

FIG. 1. The function $\zeta^{-2}(s)$, plotted against s^2. The solid curve has been computed from a nine-term truncated series. The dashed line has been obtained from the asymptotic solution in Eq. (24). The dotted curve has been drawn to join the solid and dashed portions smoothly.

series with delta-square processing (solid curve) and the result obtained from the asymptotic solution (dashed line). These have been connected graphically (dotted curve).

For a more precise connection between these two computed curves, a power-series solution of the form

$$\zeta^2(A+t)=E[1+(e_1t+e_2t^2+e_3t^3+\cdots)] \tag{25}$$

could be used, where

$$t=s-A\,. \tag{26}$$

This is a series solution centered about the displaced position $s=A$, where A can be chosen to lie in an intermediate position where interpolation between the solutions (19) and (24) is most uncertain.

The same procedure which has been used here for the solution of (18) can be used for the solution of the radial integral equation which arises when a less idealized, more realistic quasar model is analyzed.

Three integral expressions will be of importance, and are defined by

$$F_1(s)=\int_{s''=0}^{s''=s}\zeta^2(s'')s''ds''\,, \tag{27}$$

$$F_2(s)=\frac{1}{s}\int_{s''=0}^{s''=s}\zeta^2(s'')s''^2ds''\,, \tag{28}$$

$$F_3(s)=\frac{1}{s}\int_{s''=0}^{s''=s}\zeta^3(s'')s''^2ds''\,. \tag{29}$$

When the power-series expansions (19) and (21) are used, these three functions are given by

$$F_1(s)=\tfrac{1}{2}C_0s^2+\tfrac{1}{4}C_2s^4+\tfrac{1}{6}C_4s^6+\cdots, \tag{30}$$

$$F_2(s)=\tfrac{1}{3}C_0s^2+\tfrac{1}{5}C_2s^4+\tfrac{1}{7}C_4s^6+\cdots, \tag{31}$$

$$F_3(s)=\tfrac{1}{3}D_0s^2+\tfrac{1}{5}D_2s^4+\tfrac{1}{7}D_4s^6+\cdots. \tag{32}$$

From (18), (27), and (28) it is evident that

$$-\log_e\zeta^2(s)=2F_1(s)-2F_2(s)\,. \tag{33}$$

In power-series form, based on (19), this gives

$$-\log_e\zeta^2(s)=\tfrac{1}{3}C_0s^2+\tfrac{1}{10}C_2s^4+\tfrac{1}{21}C_4s^6+\cdots. \tag{34}$$

Generalizations to a more realistic quasar model, in which the intrinsic density ρ will itself depend upon radial distance, can be treated in a similar way if this dependence is expressed as a polynomial function whose coefficients are chosen to satisfy particular requirements specified in the generalized model.

IV. SURFACE RED SHIFT

With the Yilmaz exponential metric, the gravitational red shift is given by $z=e^u-1$, where u is the gravitational potential at the location of the emitting atom. If this atom is at the surface of the spherical matter distribution in the preliminary quasar model, then the gravitational red shift is given by

$$\begin{aligned} z&=(\lambda_{\text{red-shifted}}-\lambda_{\text{lab}})/\lambda_{\text{lab}}\\ &=e^{u(R)}-1\\ &=e^{F_2(S)}-1\,. \end{aligned} \tag{35}$$

Figure 2 gives this surface red shift, z, as a function of the parameter S, defined in (16). This parameter is dimensionless, but increases with the amount of matter and degree of compaction of the spherical mass distribution.

The solid portion of the curve in Fig. 2 was computed from the series expansion (31), with delta-square processing of a nine-term truncated series. The dashed portion of the curve was computed from the asymptotic solution (24). The limiting red shift for very large S is given by

$$z_\infty=e-1=1.718\,. \tag{36}$$

It is evident from Fig. 2 that the surface red shift from the gravitationally compacted sphere is not monotonic as a function of the parameter S. The red shift increases to a maximum at about $z=2.5$, then drops back toward the asymptotic value (38). This doubling back tends to emphasize the red-shift values between $z=1.7$ and $z=2.5$.

The red-shift cutoff near $z=2.5$ and the emphasis on the red-shift values near $z=2$ are features of the experimentally observed red-shift distribution for the quasars. Figure 3 shows a histogram of the red shifts of 151 quasars, assembled from the listings by Burbidge[10] and Schmidt.[11] Qualitatively there is a reasonably good correspondence between the implications of the theoretical red-shift curve in Fig. 2, and the observed distribution shown in

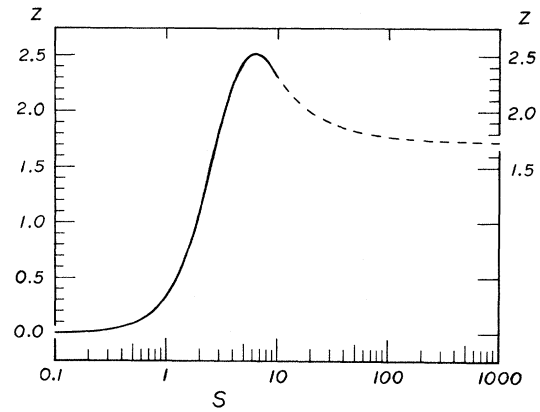

FIG. 2. The red-shift factor z, shown as a function of the parameter S.

Fig. 3. However, this is not sufficient to establish that the quasars are compacted mass concentrations with large gravitational red shifts, though this possibility is left open by the analysis which has been carried out.

While there have been additional quasar red shifts observed since these listings were compiled, including a few red shifts greater than $z = 2.5$, the histogram in Fig. 3 is a substantial and perhaps a representative sample. The fine structure in this histogram has been correlated with observational selection effects[12] arising out of the difficulty of measuring the prominent quasar emission lines when these are shifted to the vicinity of the strong emission lines from our night-sky atmosphere. However, it is possible that the strong peak near $z = 2$, and the broad maximum near $z = 0.5$, are both to be associated with characteristics of the quasar population.

The calculated red-shift curve in Fig. 2 has two branches, the main branch with $S < 6.5$ and the upper branch with $S > 6.5$. To facilitate comparison with observation, Fig. 4 is a modified histogram in which the high-red-shift quasars have been divided arbitrarily into two categories, presumed main-branch quasars and presumed upper-branch quasars. We will return to this comparison after examination of certain properties, in addition to the surface red shift, which characterize the theoretical model.

V. PHYSICAL PARAMETERS

As more matter is added to the spherical model with the intrinsic density ρ held constant, the radius of the sphere first increases, then decreases as the gravitational compaction collapses the structure to a minimum size, and finally the radius increases again toward a limiting value. This behavior of the model is shown in Fig. 5. What is plotted is

$$R/R_0 = Se^{-F_1(S)}, \tag{37}$$

where R_0 is defined by

$$R_0 = c(4\pi G\rho)^{-1/2}, \tag{38}$$

and where the function $F_1(S)$ is defined in (27), with the series expansion (30). The solid, dashed, and dotted curves have the same meaning as in Fig. 1.

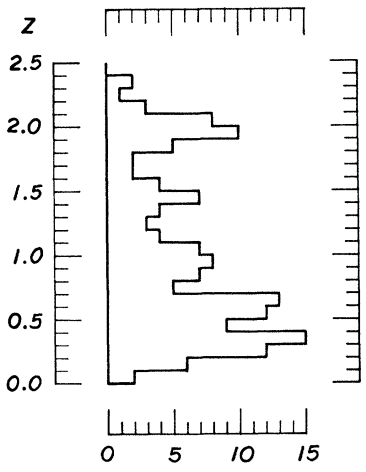

FIG. 3. Histogram showing the distribution of red-shift values for 151 quasars. The red shift z is plotted vertically, while the number of quasars in each interval, $\Delta z = 0.1$, is plotted horizontally.

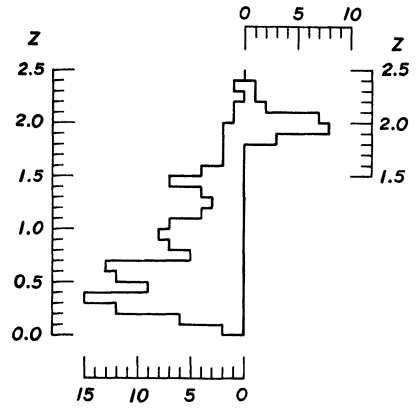

FIG. 4. Histogram showing 151 quasar red shifts, separated arbitrarily into main-branch quasars, plotted to the left of the vertical centerline, and upper-branch quasars, plotted to the right of the centerline. The upper-branch quasars, with red shifts between $z = 1.7$ and $z = 2.5$, are tentatively associated with the portion of the curve in Fig. 2 which lies to the right of the peak, in the region where S is greater than 6.5.

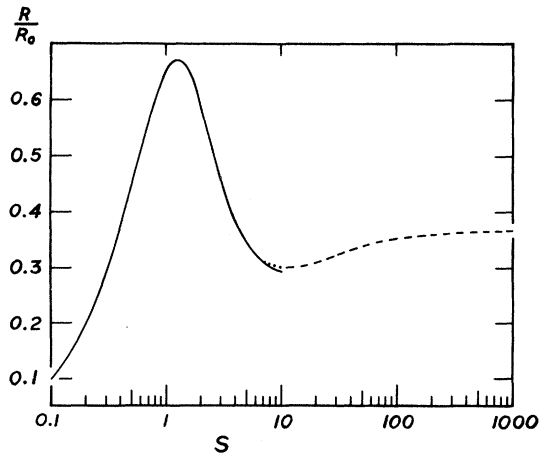

FIG. 5. The quasar radius, R, in units of R_0, shown as a function of S.

Figure 6 shows how the intrinsic mass in the spherical distribution increases as a function of S, with ρ held fixed. The plotted function is

$$M/M_0 = SF_3(S), \tag{39}$$

with M_0 defined by

$$M_0 = c^3 G^{-3/2}(4\pi\rho)^{-1/2}. \tag{40}$$

The intrinsic mass is defined by

$$M = \int_{r''=0}^{r''=R} 4\pi\rho e^{3u(r'')} r''^2 dr'', \tag{41}$$

and is proportional to the actual number of nucleons contained in the spherical mass distribution. The apparent gravitational mass, on the other hand, will incorporate the gravitational red-shift factor e^{-u}, and will be defined by

$$M' = \int_{r''=0}^{r''=R} 4\pi\rho e^{2u(r'')} r''^2 dr''. \tag{42}$$

Figure 7 is a plot of

$$M'/M_0 = SF_2(S)e^{-F_1(S)}, \tag{43}$$

with M_0 as given above in (40).

From a comparison of Fig. 6 and Fig. 7, we can see that the compacted spherical matter distribution is acting as a "gray hole," for $S > 3$. The addition of further matter, which increases the intrinsic mass M, will actually reduce the apparent mass M', weakening its gravitational pull on other matter in the vicinity.

VI. QUASAR STATISTICS

Because of this "gray hole" feature of the model, apparent in Figs. 6 and 7, we can envisage a process of galactic evolution in which matter collects

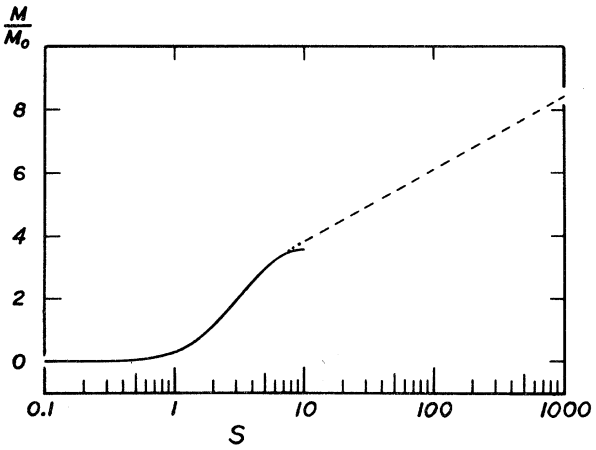

FIG. 6. The intrinsic quasar mass, M, in units of M_0, shown as a function of S. The solid, dashed, and dotted portions of the plotted function have the same meaning that they had in Fig. 1.

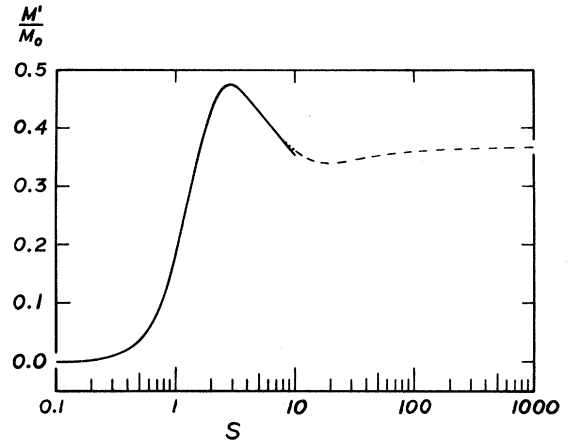

FIG. 7. The apparent quasar mass, M', in units of M_0, shown as a function of S.

by gravitational accretion, until the mass and density reach the gray-hole stage. The aggregation then weakens in its pull on further matter, but continues to increase in its intrinsic density until it reaches a density at which thermonuclear reactions begin. The quasar then becomes a visible source of electromagnetic radiation, and the energy generated is very great, so that the structure expands, evolving into a compact galaxy and then into a normal galaxy.

The core of the galaxy could retain certain quasarlike characteristics. If the galaxy is very large, explosive events in this core could eject compacted matter which was then separately visible as a smaller quasar which proceeded to evolve into a relatively small galaxy, a companion to the larger galaxy.

There would then be a distribution of quasars of different intrinsic masses, and these would be further distributed with respect to their values of intrinsic density, according to their stages of development between the quasar ignition point and the expansion into an ordinary galaxy.

We can use the monotonic curve of Fig. 6 to replace the dimensionless parameter S by the quantity

$$M/M_0 = Mc^{-3}G^{3/2}(4\pi\rho)^{1/2} \tag{44}$$

as the independent variable against which the quasar-model physical parameters are plotted. The red-shift factor z, shown earlier in Fig. 2, then takes the functional form which is graphed in Fig. 8.

It is evident from Fig. 8 that the main-branch portion of the red-shift curve, when plotted against (M/M_0), is very close to a straight line over the red-shift range from $z = 0.2$ to $z = 2.0$. For the up-

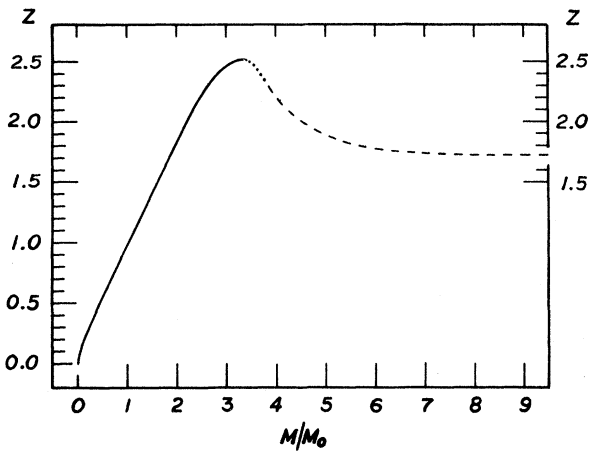

FIG. 8. The quasar red shift, z, shown as a function of the intrinsic quasar mass, M, in units of M_0.

per branch, on the other hand, the curve is very nonlinear.

Without a more specific model for quasar ignition and evolution, we cannot say how a population of quasars will be distributed over the curve of Fig. 8, except that we might expect to see a substantial number where the upper-branch portion of the curve flattens out and becomes almost horizontal. This number will be somewhat reduced if the ignition points occur only part way out along the flattened upper-branch curve.

For the translation from a particular population of quasars, distributed in surface red shift, into a predicted statistical red-shift distribution for an observationally selected listing such as that depicted in Figs. 3 and 4, we need to allow for those observational factors which may have influenced the selection process. The role of the night-sky emission lines has already been considered.[12] Many quasars have been first observed through their radio emission, while others have been studied because of their strong ultraviolet emission. Quasars are also strong emitters in the infrared.

It is difficult to draw any general conclusions about the spectral distribution of quasar emission, except to say that the distribution is very broad, and varies from one quasar to the next.[13] We can certainly say that the brighter quasars are most likely to be observed and appear in a particular listing, but we cannot use a particular black-body curve to determine the emissivity of the quasar surface as a function of emitted wavelength or red-shifted wavelength.

What we can do is to isolate the more straightforward factors that will be influencing the selection process, to see what then remains to be explained by spectral distribution functions or evolutionary processes.

We will assume therefore that the visible surfaces of the quasars are composites, containing protostars of various temperatures, in accordance with the presumed role of a quasar as a protogalaxy. The rate of emission will be slowed by the time dilation factor, $(1+z)^{-1}$, but will otherwise be proportional to the quasar surface area, $4\pi R^2$. The apparent luminosity of a quasar will depend on its distance from the observer, through the factor $r^{-2}e^{-\alpha r}$, where α is the attenuation factor resulting from intergalactic absorption. If we neglect this factor, because of our uncertainties as to the distances to the quasars, then we can compute the relative probability of observing a quasar characterized by a particular value of S, as influenced by the dependence of its radius upon S (Fig. 5) and the dependence of its red shift upon S (Fig. 2). The result is the visibility function,

$$V_B(S) = (R/R_0)^3(1+z)^{-3/2}$$
$$= S^3 \exp[-3F_1(S) - \tfrac{3}{2}F_2(S)], \qquad (45)$$

which has been made dimensionless through the inclusion of the factor R_0^{-3}. Since this factor involves the intrinsic density, ρ, which will be changing as the quasar evolves toward a compact galaxy, we cannot expect the function (45) to explain the quasar statistics fully, but only to show the effect of the quasar radius in the region (shown in Fig. 5) where that radius is changing rapidly with S.

Figure 9 shows the visibility function (45) multiplied by a normalization factor of 100 and plotted against the surface red shift z. The histogram of

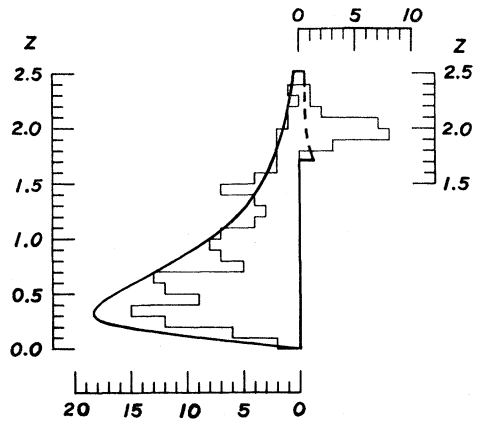

FIG. 9. A plot of 100 $V_B(S)$, where $V_B(S)$ is the visibility function in Eq. (45), against the red-shift factor z. The coordinates are those used for the histogram in Fig. 4, and this histogram has been superimposed here to show the close match along the main branch of the red-shift distribution.

Fig. 4 is superimposed, and it is evident that the part of the function where R is changing rapidly gives a fairly close match to the main-branch portion of the observed histogram.

Figure 10 shows a similar comparison, but here the function (45) has been divided by the slope of the curve in Fig. 8, in order to give additional weight to the parts of the upper branch where z is changing very slowly with (M/M_0). This is about as far as we can go, without carrying out a much more elaborate theoretical analysis, using a more sophisticated model, together with a processing of the observed data to incorporate distance estimates and associated corrections for the cosmological red shifts attributable to those estimated distances.

VII. EXAMPLES

Because of the extreme simplicity of the static-limit spherical model with constant intrinsic density, we should not expect to find that there is a precise match between this model and the observed quasars. However, the rough agreement shown in Figs. 9 and 10 is encouraging, and is a temptation leading us to look at some special cases.

In the tabulation by Burbidge[10] there are three closely spaced red shifts, with values for z of 1.800, 1.805, and 1.810. These may represent quasars close to ignition, lying on the upper branch of the quasar distribution. Specifically, we can look at the case

$$z = 1.800, \tag{46a}$$

$$S = 67. \tag{46b}$$

If we choose as the mass M the mass of our own galaxy,

$$M = 2.2\times10^{44}\,\mathrm{g}, \tag{46c}$$

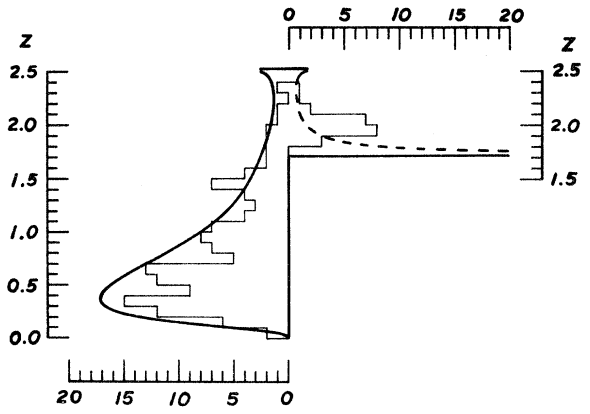

FIG. 10. A plot of 88 $V_B(S)\,|d(M/M_0)/dz|$ against the red-shift factor z, with the histogram of Fig. 4 superimposed.

we can solve for

$$\rho = 1.3\times10^{-4}\,\mathrm{g/cm^3}, \tag{46d}$$

$$R = 1.0\times10^{15}\,\mathrm{cm}, \tag{46e}$$

$$M' = 0.14\times10^{44}\,\mathrm{g}. \tag{46f}$$

The degree of gravitational self-shielding is indicated by the ratio

$$M'/M = 0.064. \tag{47}$$

The density (46d) is close to the mean density in a supergiant star of spectral classification $A5$, in the tabulation by Allen.[14] The optical appearance of such a quasar might be expected to correspond to the optical appearance of a young supergiant star. With this intrinsic density as the average over the interior of the spherical matter distribution, it is not unreasonable to expect nuclear burning, similar to that in a supergiant star, to be taking place in the core of the quasar, or in locally dense nodules distributed through the quasar.

The radius (46e) is larger than that of a single supergiant star. It is about eighteen times the radius of the largest supergiant category listed by Allen,[14] the category with spectral classification $M2$. However, on a photographic plate an object with the characteristics (46), at the distance of a galaxy, would have a stellar appearance, even though it contained enough matter to form a galaxy.

The example considered above was a highly compacted distribution with a large value of the parameter S and a large red shift. We can also consider examples for which the evolution of the quasar has reduced its intrinsic density and moved it down the main branch toward relatively small values of z.

Greenstein and Schmidt[15] have assembled and analyzed some very detailed measurements on the quasars 3C48 and 3C273. We can look at the preliminary theoretical model to see where these two quasars would fit, on the assumption that each is a protogalaxy.

For 3C48 the measured red shift is

$$z = 0.367, \tag{48a}$$

which gives, from Fig. 2,

$$S = 1.06. \tag{48b}$$

The choice (46c) for the intrinsic mass leads to

$$\rho = 3.6\times10^{-7}\,\mathrm{g/cm^3}, \tag{48c}$$

$$R = 3.6\times10^{16}\,\mathrm{cm}, \tag{48d}$$

$$M' = 1.5\times10^{44}\,\mathrm{g}. \tag{48e}$$

Since galaxies differ in size, a different choice for M could be made, within the framework of this very simple model, and the effect of choosing a larger M will be indicated later.

The emission lines from 3C48 are observed to be sharp, and Greenstein and Schmidt[15] inferred from this that the line emission comes from a gaseous layer whose thickness is only 1.6% of the quasar radius, if the observed red shift is assumed to be primarily gravitational in origin. The observed spectrum contains forbidden lines, and from the intensity of these lines, Greenstein and Schmidt estimated the electron density in the line-emitting layer to be

$$N_e = 10^5\,\mathrm{cm}^{-3}. \tag{49}$$

From the observed brightness of the hydrogen emission line $H\beta$, together with the observed line widths, Greenstein and Schmidt obtained the relationship

$$\frac{N_e^2 R^3}{r^2} = 2.8\times 10^{13}\,\mathrm{cm}^{-5}, \tag{50}$$

where r is here the distance from the quasar to the observer. Substitution then leads to the result

$$r = 1.30\times 10^{23}\,\mathrm{cm} = 42\,\mathrm{kpc}. \tag{51}$$

This is the distance obtained for 3C48 from the simple model, on the assumption that the total intrinsic mass in the model equals the mass (46c) of our own galaxy.

If instead we assume the same model but with three times the mass of our galaxy, we obtain for the red shift (48a) the model characteristics

$$\rho = 4.0\times 10^{-8}\,\mathrm{g/cm}^3, \tag{52a}$$

$$R = 1.08\times 10^{17}\,\mathrm{cm}, \tag{52b}$$

$$M' = 4.44\times 10^{44}\,\mathrm{g}, \tag{52c}$$

where the assumed intrinsic mass is now

$$M = 6.6\times 10^{44}\,\mathrm{g}. \tag{52d}$$

The distance from quasar to observer is now, for this model,

$$r = 6.7\times 10^{23}\,\mathrm{cm} = 220\,\mathrm{kpc}. \tag{52e}$$

Because of the preliminary nature of the quasar model, the results should be considered as order-of-magnitude estimates only. Furthermore, what is being examined is the role of gravitational compaction, considered separately from other factors which would enter into a more realistic model for a quasar. What we can conclude, therefore, is only that the quasar 3C48 may be a protogalaxy which is a member of our local group of galaxies.[16]

Greenstein and Schmidt[15] also considered the quasar 3C273, obtaining the relationship

$$\frac{N_e^2 R^3}{r^2} = 4.9\times 10^{14}\,\mathrm{cm}^{-5}, \tag{53}$$

and the electron density

$$N_e = 10^7\,\mathrm{cm}^{-3}. \tag{54}$$

From the measured red shift

$$z = 0.158, \tag{55a}$$

the simple spherical model gives

$$S = 0.69. \tag{55b}$$

As earlier, we can assume the intrinsic mass to equal (46c), the mass of our galaxy, and we then obtain

$$\rho = 4.0\times 10^{-8}\,\mathrm{g/cm}^3, \tag{55c}$$

$$R = 9.0\times 10^{16}\,\mathrm{cm}, \tag{55d}$$

$$M' = 1.8\times 10^{44}\,\mathrm{g}. \tag{55e}$$

Substitution into (53) leads to the distance estimate

$$r = 1.22\times 10^{25}\,\mathrm{cm} = 4.0\,\mathrm{Mpc}. \tag{56}$$

As with 3C48, the assumption of a larger intrinsic mass would lead to a larger distance estimate. The estimate (56) is thus an order-of-magnitude estimate for the distance of the quasar 3C273, and places it among the brighter galaxies[17] outside the local group.

VIII. CRITICAL DISCUSSION

The quasar model which has been examined here is obviously oversimplified in many ways. The simple spherical matter distribution, with constant intrinsic density and with a sharp outer boundary, does not make allowance for pressure and temperature variations within the distribution, or for rotational effects which must play a large role in the evolution of galaxies, particularly spiral galaxies such as our own.

On the other hand, the close correspondence between the quasar red-shift statistics and the theoretical results, as illustrated in Fig. 10, suggests that the gravitational red shift is the principal contributor to the observed quasar red shifts, and that the Yilmaz exponential metric should be used instead of the Schwarzschild metric, for calculations involving strong gravitational fields. For weaker gravitational fields, such as are found within the solar system, these two metrics give the same results.[1]

The quasar model being discussed will lead to a very large gravitational potential in the interior of a sphere with a large value of S. Figure 11 shows the red shift for a photon which leaves the center

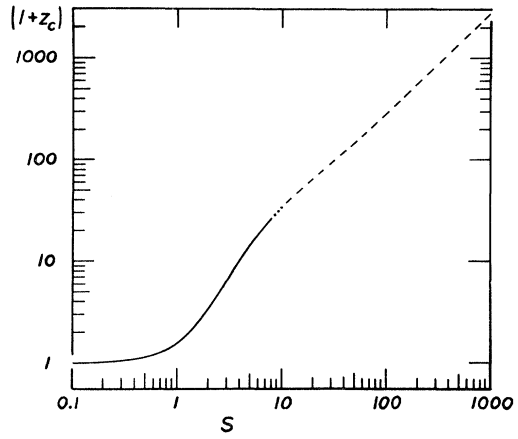

FIG. 11. A plot of $(1+z_c)$ against S, where z_c is the red-shift factor associated with radiation emitted from a protostar at the center of the quasar structure characterized by S. Here $(1+z_c)=e^{F1(S)}$.

of the sphere and is able to make its way through the interior and out past the outer boundary of the sphere. Should there not be some observational consequence which will provide evidence for this extremely compacted state of matter?

Such evidence may indeed be at hand. Many quasars do emit a very substantial fraction of their radiation in the infrared region of the spectrum. An examination of the ratio of far-infrared radiation to optical radiation, for quasars with red shifts in the vicinity of $z=2$, may disclose a bipolar statistical distribution, which could permit us to separate those quasars in the upper-branch part of the statistical distribution from the quasars in the main branch which have comparable red shifts.

The evidence assembled by Arp[6] shows a progression from quasars to compact galaxies to companion galaxies to ordinary galaxies. The close association of members of this progression having different red shifts shows that these red shifts cannot be entirely cosmological, except perhaps for the ordinary galaxies.[18] In the other members there can be a gravitational contribution to the red shift. This contribution is strongest for the quasars, which are the most compact of the members of this progression.

This ordering of galaxies and protogalaxies by compactness is also an ordering by noncosmological red shift. The evidence of this correlated ordering constitutes a fifth test of a gravitational theory.

As we have shown here, the Yilmaz exponential metric, as applied to a compacted spherical mass distribution containing a galactic amount of matter, passes this fifth test. Other gravitational theories will have to confront this fifth test, sooner or later. To the writer's knowledge, other gravitational theories have been unable to give gravitational red shifts approaching $z=2$, as appears to be necessary for this fifth test. However, there is no clear agreement on the limiting gravitational red shift available with the Schwarzschild metric.[15]

As noted earlier, the fine structure of the quasar red-shift distribution is well correlated with the observational limitations imposed by the presence of night-sky emission lines obscuring parts of the quasar spectra.[12] The gross structure of the quasar red-shift distribution is well correlated with the effects of gravitational compaction, as shown in Fig. 10, provided the Yilmaz exponential metric is used in the analysis. The model used is inadequate, however, to account for the polarization of the quasar continuum radiation, the rotational features of galaxies, particularly spiral galaxies, and the bands of galaxies observed in galactic clusters.[18] There are also special cases of quasars with $z>2.5$, and there are sure to be new observational surprises as quasars and galaxies are studied in further detail.

A more realistic quasar model, incorporating internal rotations and more flexible density distributions, is clearly needed, but can be based on the simple static model presented here, in order to retain the agreement with observation which is shown in Fig. 10. There is also qualitative agreement between the distances inferred from Arp's data[6] and the distances obtained from the simple model; and qualitative agreement between the observed variability of quasar emission[19] and the quasar radii inferred from the simple model, as illustrated in (46e), (48d), (52b), and (55d).

ACKNOWLEDGMENTS

This article represents a progress report on a long-range program. The program was supported in 1950 through an AEC Postdoctoral Fellowship at Massachusetts Institute of Technology, and in 1951 through an appointment at the MIT Laboratory for Nuclear Science and Engineering. During 1952–54 the program was supported by the U. S. Office of Naval Research, through Contract No. Nonr-778(00). Later support was provided by a Research Corporation grant in 1969.

While the writer was led to the exponential metric by a route different from that taken by Yilmaz, the writer is very grateful to Huseyin Yilmaz for recent discussions which have been valuable and very helpful.

The writer would like to express his gratitude to Sachiko Tsuruta and Evelyn W. Mack for collabora-

tive assistance during the basic work on the integral equation (18) and its solution. Luc Huang also joined in that collaboration, and was more recently working on an improved solution of the integral equation (18) at the time of his tragic death in June, 1971.

For the impetus to reconsider established or conventional theories, particularly general relativity with its very limited experimental basis, the writer is indebted to his Harvard teachers, including particularly S. A. Goudsmit, P. W. Bridgman, and W. H. Furry. Further encouragement came from Francis L. Friedman, David Finkelstein, Randal M. Robertson, Wayne R. Gruner, and Edwin B. Wilson. Steady support in recent years has come from Harvey Brooks and Gerald Holton. The writer has had valuable discussions on quasar observations and analysis with David Layzer, Philip Morrison, A. G. W. Cameron, and J. Craig Wheeler. The writer is also grateful to Sidney Coleman for help in confronting the formal problems raised by the Yilmaz theory, and to Halton C. Arp for a stimulating correspondence.

---

[1]H. Yilmaz, Phys. Rev. 111, 1417 (1958).

[2]H. Yilmaz, Phys. Rev. Letters 27, 1399 (1971).

[3]C. M. Will and K. Nordtvedt, Bull. Am. Phys. Soc. 17, 141 (1972).

[4]William Kinnersley (private communication).

[5]R. Tolman, *Relativity, Thermodynamics, and Cosmology* (Oxford Univ. Press, New York, 1934), p. 205.

[6]H. Arp, Science 174, 1189 (1971).

[7]H. C. Arp, E. M. Burbidge, C. D. Mackay, and F. A. Strittmatter, Astrophys. J. 171, L41 (1972).

[8]See *International Dictionary of Applied Mathematics*, edited by W. F. Freiberger (Van Nostrand-Reinhold, Princeton, N. J., 1960), p. 221.

[9]A. S. Householder, *The Numerical Treatment of a Single Nonlinear Equation* (McGraw-Hill, New York, 1970), pp. 135–139.

[10]E. M. Burbidge, in *Annual Review of Astronomy and Astrophysics*, edited by B. L. Goldberg (Annual Reviews, Palo Alto, Calif., 1967), Vol. 5, pp. 399–452.

[11]M. Schmidt, in *Annual Review of Astronomy and Astrophysics*, edited by B. L. Goldberg (Annual Reviews, Palo Alto, Calif., 1969), Vol. 7, pp. 527–552.

[12]R. C. Roeder and C. C. Dyer, Nature Phys. Sci. 235, 3 (1972).

[13]G. Burbidge and M. Burbidge, *Quasi-Stellar Objects* (W. H. Freeman, San Francisco, 1967), p. 51.

[14]C. W. Allen, *Astrophysical Quantities*, 2nd ed. (The Athlone Press, Univ. of London, London, 1964), p. 203.

[15]J. L. Greenstein and M. Schmidt, Astrophys. J. 140, 1 (1964).

[16]C. W. Allen, *Astrophysical Quantities*, 2nd ed. (The Athlone Press, Univ. of London, London, 1964), p. 272.

[17]C. W. Allen, *Astrophysical Quantities*, 2nd ed. (The Athlone Press, Univ. of London, London, 1964), p. 273.

[18]Evidence has been assembled by W. G. Tifft [Astrophys. J. 175, 613 (1972)] of a correlation between galactic red shift and apparent core luminosity, for the galaxies in the Coma cluster. The correlation takes the form of a banded structure within the plot of core magnitude against red shift. This evidence suggests the presence of noncosmological red shifts for ordinary galaxies.

[19]See Chapter 6 of Ref. 13.